Analysing the effects of sliding, adhesive contact on the deformation and stresses induced within a multi-layered elastic solid

W. W. F. Chong[a,b,c,1] and S. J. Chidlow[d]

[a] *UTM Centre for Low Carbon Transport in Cooperation with Imperial College London, Universiti Teknologi Malaysia (UTM), Johor, Malaysia*

[b] *Faculty of Mechanical Engineering, Universiti Teknologi Malaysia (UTM), Johor, Malaysia*

[c] *National Centre for Advanced Tribology (nCATS), Faculty of Engineering and the Environment, University of Southampton, Southampton, UK*

[d] *Department of Mechanical Engineering and Mathematical Sciences, Oxford Brookes University, UK*

Abstract

This paper presents a mathematical model of sliding, adhering contact between a rigid parabolic indenter and a multi-layered elastic solid, which is assumed to comprise of a homogeneous coating bonded through a functionally-graded transitional layer to a homogeneous substrate. The adhesive forces in this investigation are modelled using Lennard-Jones potential and an iterative algorithm is proposed that solves for the contact pressure, surface displacement and sub-surface stresses resultant within the layered solid. The effects of surface adhesion and different material properties such as varying coating/transition layer thickness and coating hardness on the solution of the contact problem are subsequently investigated in detail.

The numerical approach presented in this paper demonstrates the significance of having a suitable mathematical representation for the traction distribution along the sliding, adhering contact. It is found that under weakly adhering conditions, the assumption of only Coulombic traction suffices to determine the displacements and subsurface stresses within the multi-layered

[1] *william@mail.fkm.utm.my*

solid. However, it is noted that stress concentrations within the material begin to propagate through all three layers of the elastic solid with increased surface adhesion, which could potentially induce plasticity and lead to material ploughing under sliding. The proposed model allows us to further investigate and improve our understanding of the combined effects of traction and boundary adhesion in sliding contacts, which can be used to inform the design of materials needed in such conditions.

Keywords: Lennard-Jones potential, layered solids, contact mechanics, surface adhesion, traction

---

1. Introduction

Engineering materials that possess an increased resistance to wear can be achieved by introducing controlled gradients in the materials near their surface [1]. These graded materials, known as functionally graded materials (FGMs), exhibit either continuously or discretely varying physical and mechanical properties throughout their depth, depending on the desired application [2]. The graded properties of the FGM are commonly achieved through surface modification processes such as thermal spray, physical or chemical vapour deposition and laser heat treatment. The use of FGMs as protective coatings is extremely beneficial in automotive applications such as engine cylinder liners, gears and cams, as tribological studies have shown that a significant amount of surface asperity interactions during operation can induce wear, which in turn leads to a drop in mechanical efficiency [3, 4, 5]. It is therefore crucial to be able to accurately characterise and tailor graded elastic coatings to achieve the desired tribological effects that can improve wear resistance of machine elements.

A fundamental understanding of the characteristics of FGM coatings is essential when selecting materials to suit the operating conditions of the designed machine elements. This is often achieved by first using mathematical models to investigate the effects of normal loading on the contact. In the case of a homogeneous material, the classical theory of Hertz [6] may be used to examine contact behaviour. However, with the miniaturisation of machine elements, short-ranged intermolecular forces will increase in significance, leading to boundary adhesion between opposing surfaces. Under these circumstances, researchers may instead choose to apply the JKR [7], DMT

[8] or Maugis-Dugdale [9] adhesive models to study the contact under the influence of boundary adhesion. Unfortunately FGMs are not homogeneous, which severely limits the usefulness of such classical models to investigate contact behaviour.

The use of FGMs as protective coatings means that a coated base material may be considered to be a layered solid. As an initial approximation, Teodorescu and Rahnejat [10] modelled a coated system as two perfectly bonded homogeneous layers and presented an iterative algorithm that may be used to compute the contact footprint within the material under normal loading. An alternative method was proposed by Chen *et al* [11] who used the Equivalent Inclusion Method (EIM) to model elasto-plastic indentation of layered materials. In a more recent development, Yu *et al* [12] and Wang *et al* [13] studied the frequency response functions and fretting behaviour for multilayered materials respectively, focusing on the subsurface stress propagation across the layered solid.

The studies above assumed layered solid where each layer of coating consists of homogeneous materials. For FGM coatings, the varying material properties within the graded coating may be approximated using simple mathematical functions whilst the substrate can still be considered to be homogeneous. By applying a power law to describe the graded properties within FGM layers, an analytical solution was proposed by Giannakopoulos and Suresh [14] for a non-adhering three-dimensional graded elastic medium. Guler and Erdogan [15] and Chidlow *et al* [16] consider the mechanical properties of the graded coating to vary exponentially throughout its depth and construct solutions to the contact problem under study using Fourier transform and Fourier series approximations respectively.

In addition to contact models developed for layered solids under normal loading, there have been models developed that seek to solve adhesive contact problems involving inhomogeneous materials. For an adhering elastic layered solid under normal loading, Johnson and Sridhar [17] presented an extended JKR adhesive model. In a similar investigation, Mary *et al* [18] proposed a semi-analytical model that describes the behaviour of a graded elastic layered solid within adhesive contacts. Sergici *et al* [19] applied a Maugis type adhesive model to investigate the contact between a spherical indenter and an elastic layered solid. More recently, Chidlow *et al* [20] and Chong and Chidlow [21] introduced surface adhesion via the Dugdale and Lennard-Jones potential respectively to simulate a rigid cylindrical geometry indenting a graded elastic layered solid comprising a FGM perfectly bonded

to a homogeneous substrate.

Whilst all of the models discussed above are very useful in different circumstances, they all assume that the contact involves only normal loading, which is not sufficient to understand the tribological behaviour of a moving machine element, such as the sliding of a piston ring on an engine cylinder liner or even a cam on a tappet in an engine valve train analysis. Con-tact models that seek to approximate the solution of such problems must take account of combined normal loading and sliding of the contact in or-der to provide meaningful predictions of the behaviour of the layered elastic medium. In general, contact theories for combined normal and sliding between non-adhering surfaces are well understood with the tangential sliding given by Amonton's law [22]. For example, Hamilton and Goodman [22] and Poritsky [23] analysed the case of a cylindrical and circular indenter sliding on the surface of a homogeneous elastic medium.

For FGMs, Giannakopoulos and Pallot looked at the contact behaviour of a flat and cylindrical punch on an elastic graded material subject to tangential and normal load [24]. Guler and Erdogan [25] and Ke and Wang [26] also proposed mathematical models for a selection of sliding frictional con-tact problems involving rigid indenters of various shapes and a functionally graded material. In order to better understand the performance of graded elastic layered solids in such contacts, Chidlow and Teodorescu [27] focused on characterising the influence of tangential traction induced by a cylindri-cal indenter on the subsurface stresses of a multi-layered elastic solid with an FGM transitional layer. For an adhering cylindrical indenter on a FGM, Chen *et al* [28] investigated the effects of normal and tangential on the con-tact behaviour of their selected problem.

This paper provides a thorough investigation of the effects of boundary adhesion on a rigid parabolic indenter sliding along the surface of a multi-layered elastic solid comprising a homogeneous coating bonded through a functionally-graded transitional layer to a homogeneous substrate. A previous investigation by Chidlow and Teodorescu [27] showed that when the layered solid described above experiences sliding, non-adhesive contact with a rigid parabolic indenter, the magnitude of the maximum principal stresses induced within the layered solid are highly dependent on the hardness of the coating, the friction coefficient and the coating/interlayer thickness ra-tio. It was observed that hard coatings are particularly sensitive to the coat-ing/ interlayer thickness ratio as dramatic increases in the maximum attained stress and the location at which it occurs are observed as this parameter

varies.

The work conducted within this paper uses the model derived by Chidlow and Teodorescu [27] to describe the stresses and displacements within the layered solid induced by adhesive contact between the solid and a rigid punch using the Lennard-Jones force law. A new algorithm is then derived which allows us determine how the presence of adhesion further affects the behaviour of the stresses induced within the layered solid through contact and whether the general trends observed in the case of non-adhesive contact still hold true. To the best of the authors knowledge, the algorithm presented in this work is the only model currently available that is capable of modelling such contact problems.

2. Mathematical Model

Figure 1 illustrates the simulated contact problem, which involves a normally loaded rigid cylindrical indenter sliding over the surface of a multilayered elastic medium in a state of plane strain. The solid occupies the lower half-plane bounded by $y = 0$ and is assumed to comprise of a finitely thick homogeneous coating occupying $-h_1 \leq y \leq 0$ (region 1) and FGM transition layer occupying $-h_2 \leq y < h_1$ (region 2) bonded to an infinitely deep homogeneous substrate (region 3). Within the transition layer, the material properties of the solid progressively change from those of the coating to those of the substrate. The shear modulus of the solid is then modelled as

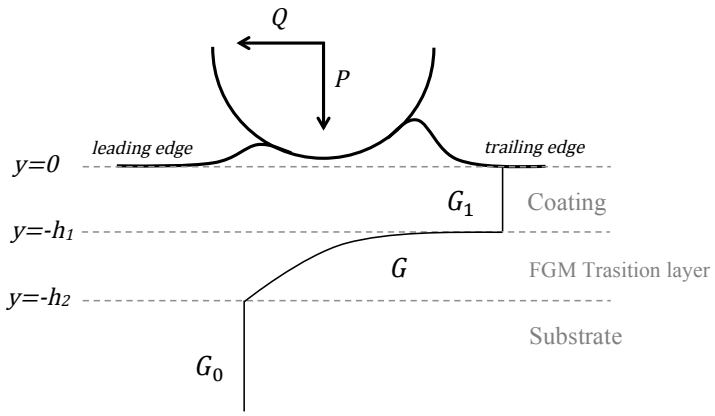

Figure 1: Schematic diagram for the investigated contact problem

$$G(y) = \begin{cases} G_1, & -h_1 \leq y \leq 0, \\ G_0 e^{\zeta(y+h_2)}, & -h_2 \leq y \leq -h_1, \\ G_0, & -\infty < y < -h_2 \end{cases} . \tag{1}$$

where

$$\zeta = \frac{1}{h_2 - h_1} ln \left(\frac{G_1}{G_0} \right),$$

which ensures that the shear modulus is continuous at the boundaries between layers. The assumption of combined normal loading and sliding of the rigid cylindrical indenter on the surface of the solid allows us to deduce the boundary conditions

$$\sigma_{yy}(x, \ 0) \ = \ -p(x) \tag{2}$$

$$\sigma_{xy}(x, 0) = -q(x) \tag{3}$$

where $p(x)$ denotes the contact pressure and $q(x)$ denotes the tangential traction. As the coating and substrate are assumed to be perfectly bonded to the interlayer, we also have the matching conditions

$$u_j(x, -h_j) = u_{j+1}(x, -h_j), \tag{4}$$

$$v_j(x, -h_j) = v_{j+1}(x, -h_j), \tag{5}$$

$$\sigma^{(j)}_{xy}(x, -h_j) = \sigma^{(j+1)}_{xy}(x, -h_j), \tag{6}$$

$$\sigma^{(j)}_{yy}(x, -h_j) = \sigma^{(j+1)}_{yy}(x, -h_j), \tag{7}$$

for $j = 1, 2$ where u_j denotes the horizontal displacement and v_j denotes the vertical displacement within each region of the solid. In real terms, these matching conditions ensure continuity of displacement and stress at each interface between regions.

In addition to the boundary and matching conditions applied here, we also insist that the following radiation conditions are fulfilled:

$$|u_j|, |v_j| \to 0, \qquad x \to \pm\infty, \tag{8}$$

$$|u_j|, |v_j| \to 0, \qquad y \to -\infty. \tag{9}$$

for $j = 1, 2, 3$. This ensures that the stresses and displacements induced within the material decay to zero far away from the contact.

It has been shown in classical studies of contact mechanics (e.g. [29]) that the stresses within the solid may be evaluated from the following indefinite integrals

$$\sigma_{yy}^{(j)} = -\frac{1}{2\pi}\int_{-\infty}^{\infty} \xi^2 \hat{\phi}_j(\xi, y) e^{-i\xi x} d\xi, \tag{10}$$

$$\sigma_{xx}^{(j)} = \frac{1}{2\pi}\int^{\infty} \hat{\phi}_j''(\xi, y) e^{-i\xi x} d\xi, \tag{11}$$

$$\sigma_{xy}^{(j)} = \frac{i}{2\pi}\int_{-\infty}^{-\infty} \xi \hat{\phi}_j'(\xi, y) e^{-i\xi x} d\xi, \tag{12}$$

where $\hat{\phi}_j(\xi, y)$, $j = 1, 2, 3$ denotes the Fourier transform of the stress function with each region of the solid, $'$ denotes differentiation with respect to y and $i = \sqrt{-1}$. The stress functions specific to the solid under study in this work were computed in Chidlow and Teodorescu [27] and are detailed in full in Appendix B.

Both the horizontal and vertical displacement of the solid may also be determined in a similar way. Consideration of Hooke's laws allows us to determine that

$$u_j(x, y) = \frac{i}{2\pi G(y)}\int_{-\infty}^{\infty} \frac{1}{\xi}\Big(\hat{\phi}_j''(\xi, y) + \xi^2 \hat{\phi}_j(\xi, y)\Big) d\xi, \tag{13}$$

$$v_j(x, y) = \frac{1}{4\pi G(y)}\int_{-\infty}^{\infty} \frac{1}{\xi^2}\Big((1-\nu)\hat{\phi}_j'''(\xi, y) - \zeta(1-\nu)\hat{\phi}_j''(\xi, y) - \xi^2(2-\nu)\hat{\phi}_j'(\xi, y) - \nu\zeta\xi^2 \hat{\phi}_j(\xi, y)\Big) d\xi \tag{14}$$

for $j = 1, 2, 3$. Full details of the quantities appearing in equations (10)-(14) and a list of all model parameters are contained in Appendix B.

3. Deriving an iterative algorithm to solve the contact problem

3.1. Formulating the Algorithm

We are interested in simulating the effects of sliding, adhesive contact between the solid surface and rigid indenter. The adhesive forces within this work are simulated using the Lennard-Jones force law. This gives the contact

pressure, $p(x)$ as

$$p(x) = -\frac{8\gamma}{3\epsilon}\left(\left(\frac{\epsilon}{h(x)}\right)^3 - \left(\frac{\epsilon}{h(x)}\right)^9\right), \tag{15}$$

where the atomic equilibrium spacing is given as ϵ and the contact gap, $h(x)$ is defined as

$$h(x) = -\alpha + \epsilon + h_c(x) + v(x,0) \tag{16}$$

The term h_c refers to the geometrical shape of the rigid indenter and the term α is defined as the indenter approach. The normal load, P, applied onto the surface of the solid can be calculated using

$$P = \int_{-\infty}^{\infty} p(x)dx. \tag{17}$$

We note here that as the applied pressure will only be non-zero in a finite width interval, this integral will be easy to evaluate.

In order to solve the contact problem, all quantities are non-dimensionalised using the transformations given in Appendix C. The applied contact pressure and contact gap in terms of the new dimensionless co-ordinates are then

$$p(X) = \frac{8}{3}\left(\left(\frac{1}{H(X)+1}\right)^3 - \left(\frac{1}{H(X)+1}\right)^9\right), \tag{18}$$

$$H(X) = -\Delta_c + H_c(X) - V(X) \tag{19}$$

with

$$H_c(X) = \left(R_x - \sqrt{R_x^2 - x^2}\right)/\epsilon. \tag{20}$$

The aim of the work is to compute the contact gap width, H, as this then allows us to calculate the applied pressure via equation (18). In order to achieve this, we rearrange equation (19) to obtain the residual function

$$R(X) = H(X) + \Delta_c - H_c(X) + V(X,0), \tag{21}$$

which will be identically zero if the exact contact pressure is used to compute the surface deflection. Minimising the residual function, $R(X)$ ensures an

accurate approximation to $H(X)$ and $p(X)$ is obtained. This idea forms the basis of the iterative algorithm used in this work.

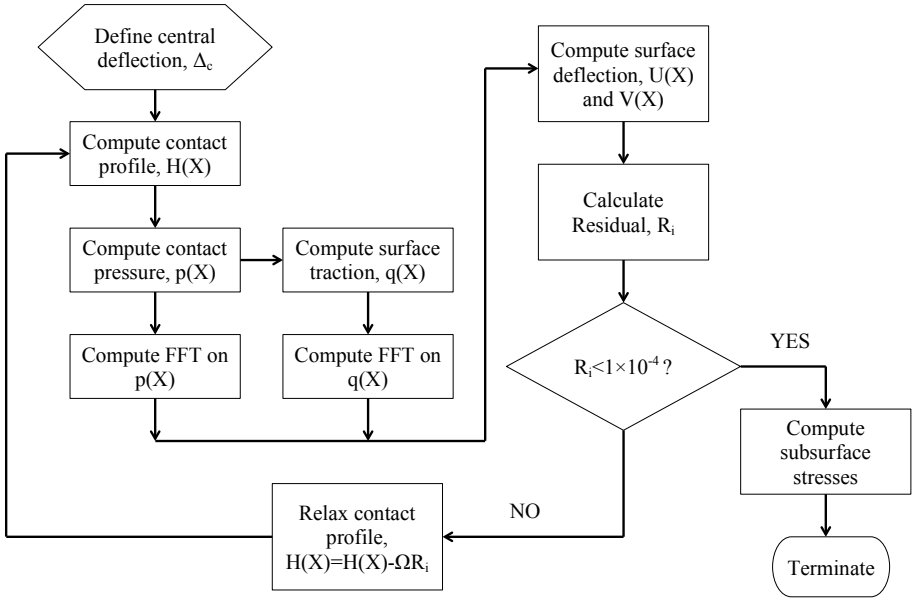

Figure 2: A flow chart of the proposed algorithm

The iterative procedure commences with an initial guess at the contact gap denoted $H_0(X)$, which is used to calculate both $P_0(x)$ and $Q_0(x)$. The dimensionless counterparts of the integrals appearing in equations (10)-(12) and (13)-(14) are then evaluated using the Fast Fourier Transform (FFT). Finally, the residual function $R_0(X)$ is calculated and the iteration is updated using the formulae

$$H_{i+1}(X) = H_i(X) - \Omega R_i(X), \tag{22}$$

for $i = 0, 1, 2, ...$ where Ω is the relaxation factor. The iterative loop is terminated when the criterion

$$max\big(R_i(X)\big) < 1 \times 10^{-4} \tag{23}$$

is met, which ensures that an accurate approximation to the contact and tangential pressures is obtained. This algorithm is summarised in figure 2, whilst a selection of possible termination criteria are summarised in Table 1.

This table shows that the termination criterion is chosen to ensure that the maximum relative error in the contact pressure is less than 0.1%

Table 1: The effects of choosing different termination criterion on the solution of the dimensionless contact pressure $p(X)$

Termination Criterion	**Simulation time (s)**	**Averaged Relative Error (%)**	**Maximum Relative Error (%)**
1×10^{-2}	317	0.491	7.541
1×10^{-3}	464	0.028	0.646
1×10^{-4}	589	0.003	0.098
1×10^{-5}	731	-	-

3.2. Evaluation of indefinite integrals

A key part of the algorithm presented here is the determination of the horizontal and vertical displacement of the solid surface and the sub-surface stresses. However, as can be seen in equations (10)-(14), these quantities are defined in terms of inverse Fourier transforms which can be only be evaluated numerically due to the complexity of the integrand.

Within this work, we use the inverse Fast Fourier Transform (IFFT) to evaluate these quantities which requires the discretisation of both the spatial and frequency variables. Hence, we let x occupy the finite interval $[-L,\ L]$ which is split into $N-1$ sub-intervals of width Δ and the frequency variable $\omega = \xi/2\pi$ occupy the finite interval $[-\omega_F, \omega_F]$. The nth and kth co-ordinates in the spatial and frequency domains are then defined to be

$$x_n = -L + (n-1)\Delta, \tag{24}$$

$$\omega_k = \frac{1}{2N\Delta}\Big(2(k-1) - (N-1)\Big) \tag{25}$$

for $n,\ k = 1,\ ...N$. This discretisation allows us to implement the classical IFFT algorithm of Cooley and Tukey [30], so N is taken to be a power of 2 here ($N = 2^\gamma$ for some integer γ). The reader is referred to [27] for a more detailed explanation of the application of the IFFT process in this context if required.

4. Results and Discussions

4.1. Verification of contact model

In order to validate this model, we initially consider only normal con-tact, so set $\eta = 0$, we compare our results against those produced using the Maugis-Dugdale adhesive model applied to a homogeneous material and coated substrate.

The Maugis-Dugdale model inherently assumes that adhesive forces are constant within two specified regions: $[-c, -a]$ and $[a, c]$ where a represents the contact half width of the Maugis-Dugdale model and c defines the outer half width of the adhesive region. The Lennard Jones potential however assumes that adhesive forces are continuous and decay to zero sufficiently far away from the contact. A basis of comparison between the two models applied to a homogeneous material was suggested by Wu [31] who used an equivalent contact half width for the Lennard Jones model, given by the formula

$$b = a + 0.4(c - a), \tag{26}$$

which was originally derived by Lantz *et al* [32]. We also use this approach here to compare model predictions and assume that the contact half width for the Lennard-Jones force law occurs at the minimum point of the pressure distribution.

Figures 3(a) present the results obtained using both models for a homogeneous material whilst figure 3(b) depicts the set of results obtained for a layered solid with a homogeneous coating of 50nm. Both sets of obtained results agree well and give rise to a maximum relative error in the contact pressure of 2.3% and 4.8% for the homogeneous case and coated case respectively with surface energy, $\Delta\gamma$ of $10mJ/m^2$. The obtained relative errors for the equivalent contact half widths are 2.3% and 4.1% for the homoge-nous and coated case respectively when the surface energy is increased to $20mJ/m^2$. Given that the Maugis-Dugdale model assumes an adhesive pro-file which possesses jump discontinuities whilst the Lennard Jones potential is continuous everywhere, an error of less than 5% in this comparative study is very good.

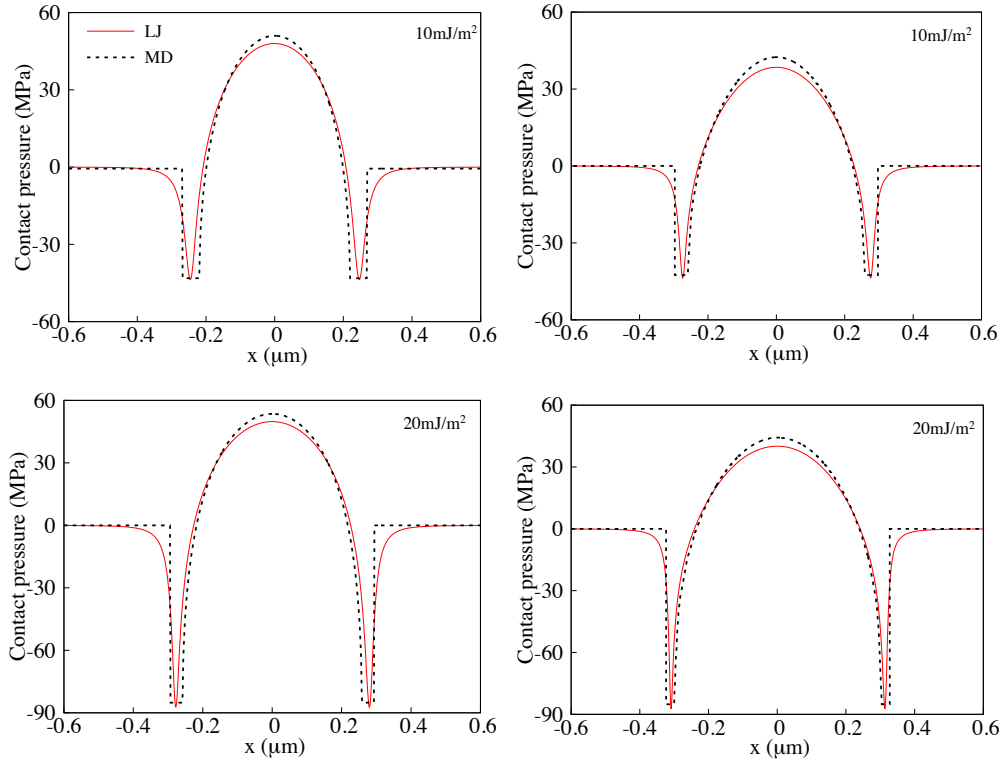

(a) Homogeneous material

(b) Single layer homogeneous coating of 50nm

Figure 3: Contact pressure distribution comparison between homogeneous material and layered solid with homogeneous coating ($\delta_{max} = 1$nm and $\eta = 0$)

4.2. Investigating the full contact problem combining adhesion and traction

We now investigate the contact characteristicics of a rigid indenter sliding over a multi-layered elastic solid (see figure 1) using the simulation parameters given in Appendix D and taking the Young's modulus of the substrate to be 25 GPa. We initially investigate the effects of boundary adhesion (coat-ing surface energy, $\Delta\gamma = 10\text{mJ/m}^2$) on the applied pressure and sub-surface stress fields. The simulated parameters are selected to ensure that the con-tact problem investigated falls within the adhesive transition region between the DMT and JKR adhesive region as described using Tabor's parameter [33]. As a first approximation, a Coulombic traction, $q(x) = \eta p(x)$ is used to describe the tangential motion, where η denotes the friction coefficient.

4.3. The effects of boundary adhesion

Figure 4(a) shows the contact pressure distribution and surface deflection for a non-adhering rigid indenter in contact with a multi layered solid, consisting of a soft coating satisfying $\mu_1/\mu_0 = 0.5$. At a maximum deflection or indentation of $\delta_{max} = 1$nm, it can be observed that the Hertzian-like peak pressure is skewed towards the trailing edge of the contact when the friction coefficient, η is increased. Similar characteristics are also observed in [25, 26, 27]. The deflection along the leading edge is observed to be higher than the trailing edge with increasing η. With the introduction of Lennard-Jones type adhesion along the contact, the layered solid is attracted towards the sides of the indenter, leading to bulging edges along the adhering region (see figure 4(b)).

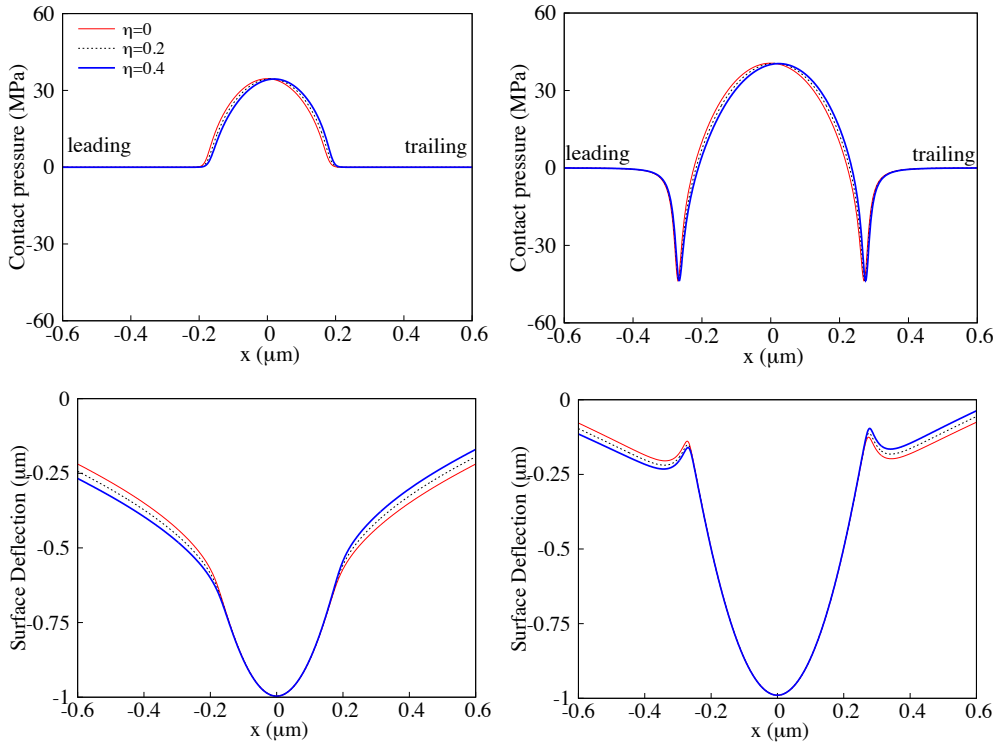

(a) Non-adhering contact (b) Adhering contact ($\Delta\gamma = 10\text{mJ}/m^2$)

Figure 4: Contact behaviour considering the effect of boundary adhesion with increasing traction for soft coating, $\mu_1/\mu_0 = 0.5$

Consideration of the contact pressure and surface deflection in isolation

describe the interfacial contact behaviour but the sub-surface stress fields must be determined to fully understand the characteristic of the contact throughout the depth of the layered solid. In this study, the maximum principal stress is computed as previous investigations by [21] and [27] have used these stresses so an easy comparison with these investigations can be made. Throughout this section, we produce results for two different types of coatings: hard ($\mu_1/\mu_0 = 2$) and soft ($\mu_1/\mu_0 = 0.5$).

Figure 5 presents the sub-surface stresses for the pressure distributions obtained for the soft coating in the previous figure. We observe that for the case of non-adhering contact, the region of highest stress obtained shifts upwards towards the trailing edge of the contact as the friction coefficient increases. This is in accord with the observation made by Chidlow and Teodorescu [27]. However, for the adhering contact, there are two distinct regions of high stress which occur. These areas move progressively towards the solid surface in the presence of increased friction and appear directly underneath the parts of the solid surface which experience only adhesive force. These areas of stress are much larger than those obtained for a non-adhering contact and could potentially initiate plasticity that might lead to material ploughing under sliding.

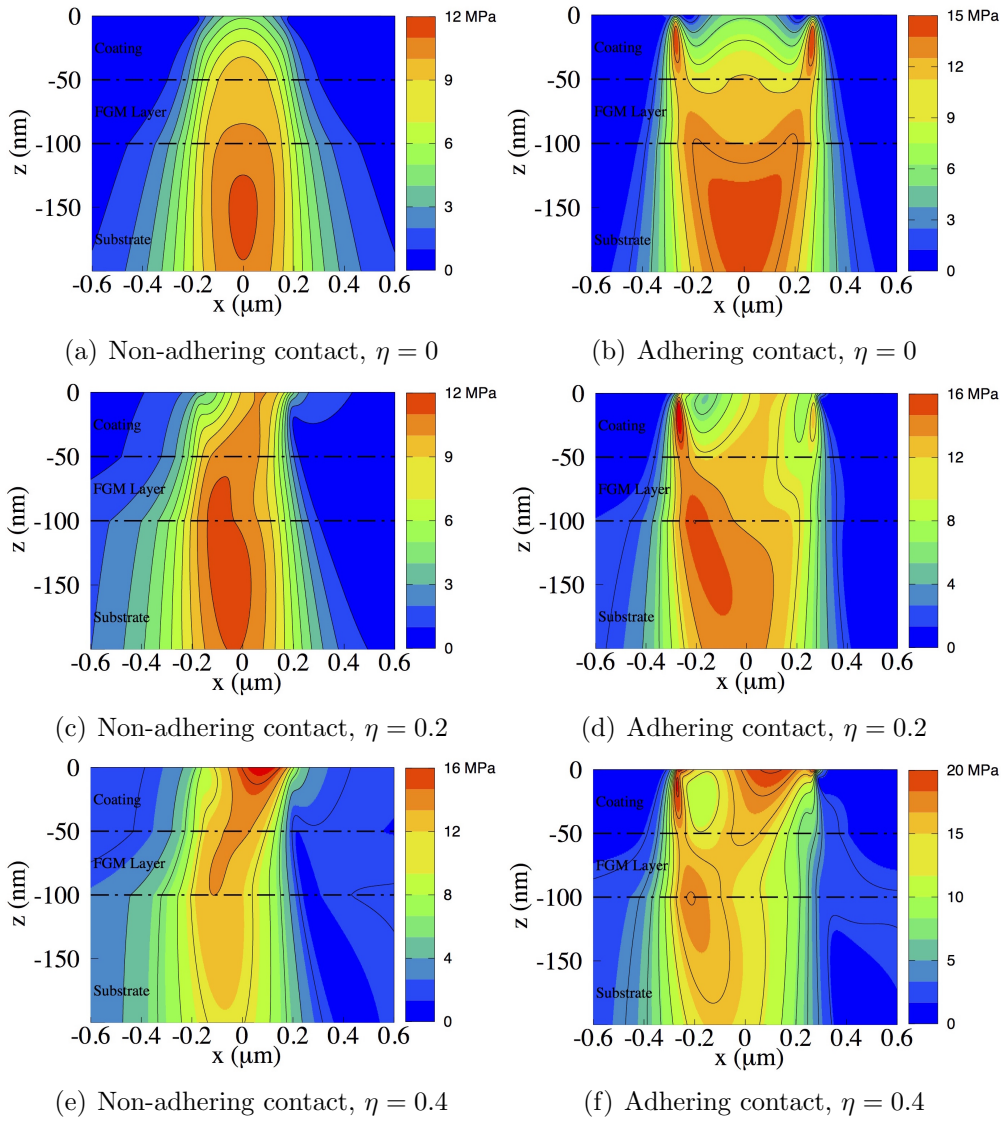

(a) Non-adhering contact, $\eta = 0$

(b) Adhering contact, $\eta = 0$

(c) Non-adhering contact, $\eta = 0.2$

(d) Adhering contact, $\eta = 0.2$

(e) Non-adhering contact, $\eta = 0.4$

(f) Adhering contact, $\eta = 0.4$

Figure 5: Sub-surface stress plots considering the effect of boundary adhesion ($\Delta\gamma = 10$ mJ/m^2) with increasing traction for soft coating, $\mu_1/\mu_0 = 0.5$

The contact pressure and surface deflection for the hard coating satisfying $\mu_1/\mu_0 = 2$ subject to the same contact conditions as the soft coating previously considered are presented in figure 6. We note in this case that the peak pressure along the contact increases for both adhering and non-adhering contacts. This is because of the increased resistance towards deflection for

the harder coating. However, the distortion of the peak pressure along the contact towards the trailing edge becomes more apparent for the harder coating as compared to the softer one when η is increased. We also note that whilst the harder coating is attracted to the sides of the indenter, there is no evidence of bulging around the edges, which does occur for the softer coating.

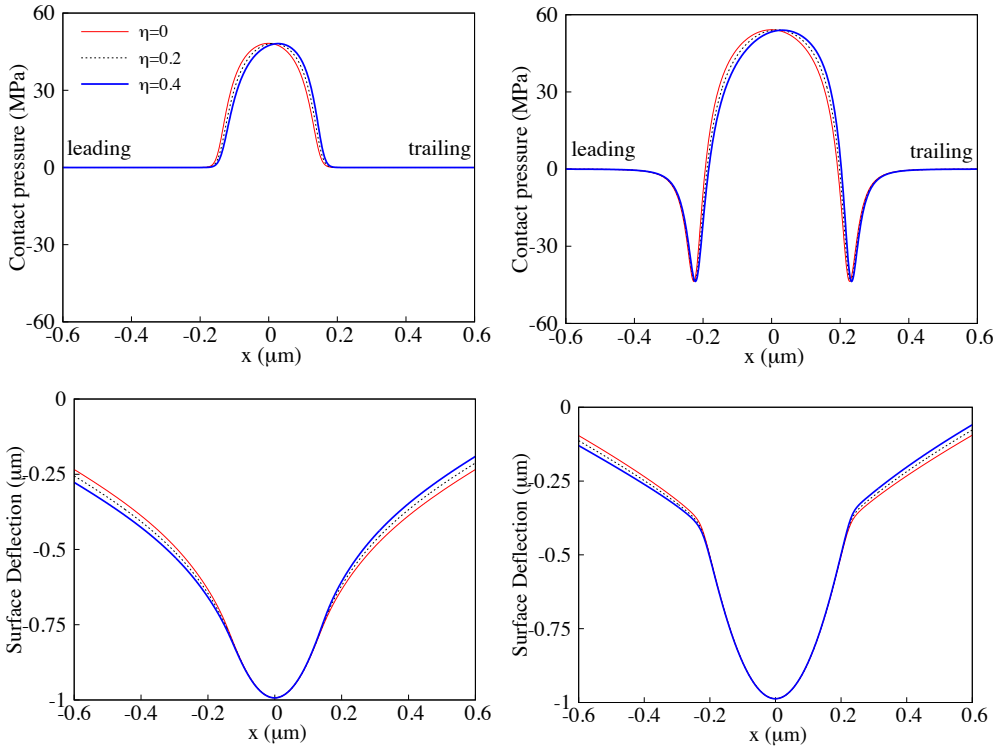

(a) Non-adhering contact (b) Adhering contact ($\Delta\gamma = 10\text{mJ}/m^2$)

Figure 6: Contact behaviour considering the effect of boundary adhesion with increasing traction for hard coating, $\mu_1/\mu_0 = 2.0$

Figure 7 depicts the subsurface stresses corresponding to the pressure curves in the previous figure. It is observed that because of the higher maximum contact pressure obtained for the harder coating, the layered solid experiences higher stresses in comparison with the softer coating. Under non-adhering conditions, the stress concentration expands towards the leading edge as the friction coefficient increases. The same is also true for adhering contacts, with the exception that the stress concentration remains within the coating or transition layer regardless of the value of η. When comparing

the observations of both hard and soft coatings bonded to an identical substrate for a given maximum deflection, the simulated results show that softer coatings tend to experience less stress and provide lower resistance to sliding, which reduces the possibility of plastic deformation occurring and leads to a possibly lower wear rate.

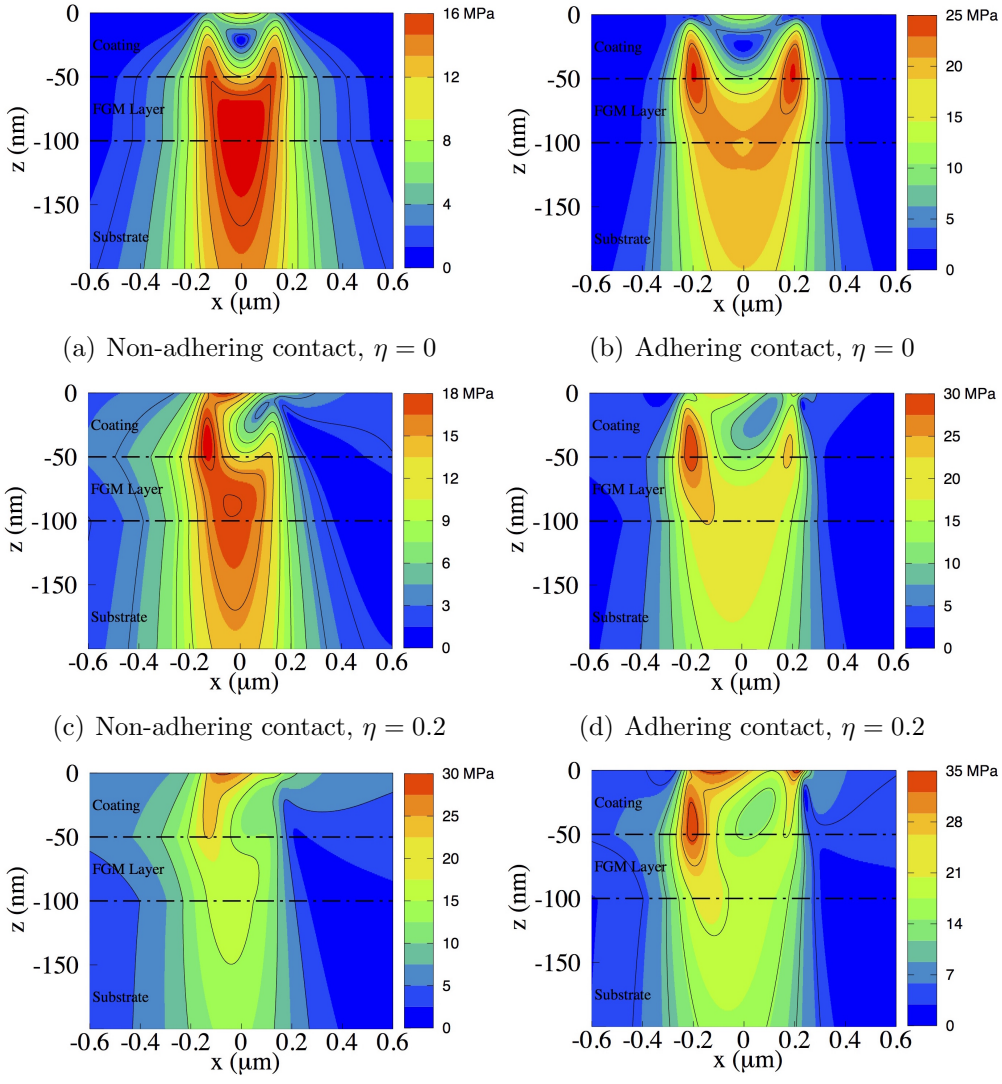

(a) Non-adhering contact, $\eta = 0$

(b) Adhering contact, $\eta = 0$

(c) Non-adhering contact, $\eta = 0.2$

(d) Adhering contact, $\eta = 0.2$

(e) Non-adhering contact, $\eta = 0.4$

(f) Adhering contact, $\eta = 0.4$

Figure 7: Sub-surface stress plots considering the effect of adhesion ($\Delta\gamma = 1.0$ J/m^2) with increasing traction for hard coating, $\mu_1/\mu_0 = 2.0$

4.4. The effects of coating thickness

We have already seen that the introduction of boundary adhesion dramatically changes the subsurface stresses within a layered solid when compared with non-adhering contacts. We now turn our attention to the effects of coating thickness on the solution of the contact problem. Figure 8 presents the predicted contact pressure obtained for three different coating thicknesses. It should be noted in each case that the interlayer thickness was taken to be a fixed constant (50nm). We observe that for a central deflection of 1nm and friction coefficient $\eta = 0.4$, the peak pressure for the soft coating reduces as the coating thickness increases, whilst the opposite is true for the hard coating. As the coating thickness is increased, it is also seen that the region of highest stress shifts upwards towards the surface in the soft coating as a result of reduced peak pressure (see figure 9). However, for the hard coating, the stress concentration propagates towards the coating/transition layer interface within the FGM layer with increased peak pressure, which could make the solid more susceptible to delamination of the coating.

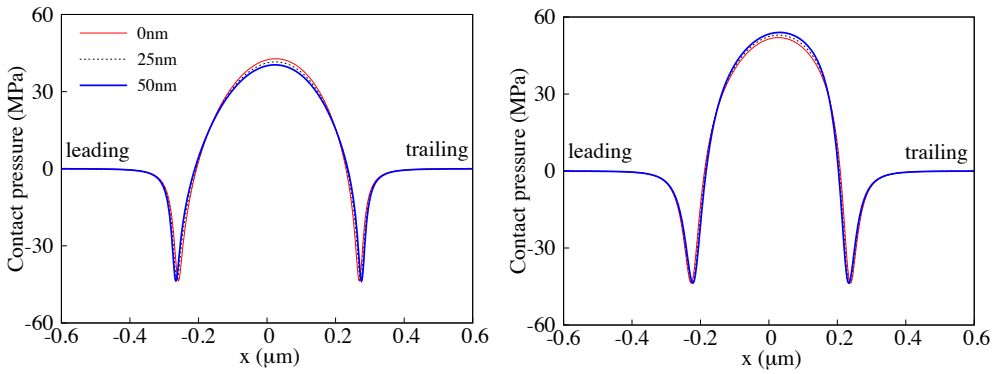

(a) soft coating, $\mu_1/\mu_0 = 0.5$ (b) hard coating, $\mu_1/\mu_0 = 2.0$

Figure 8: Contact behaviour considering coating thickness variation separated from the substrate by a 50nm thick FGM transition layer ($\Delta\gamma = 10\text{mJ}/m^2$, $\eta = 0.4$)

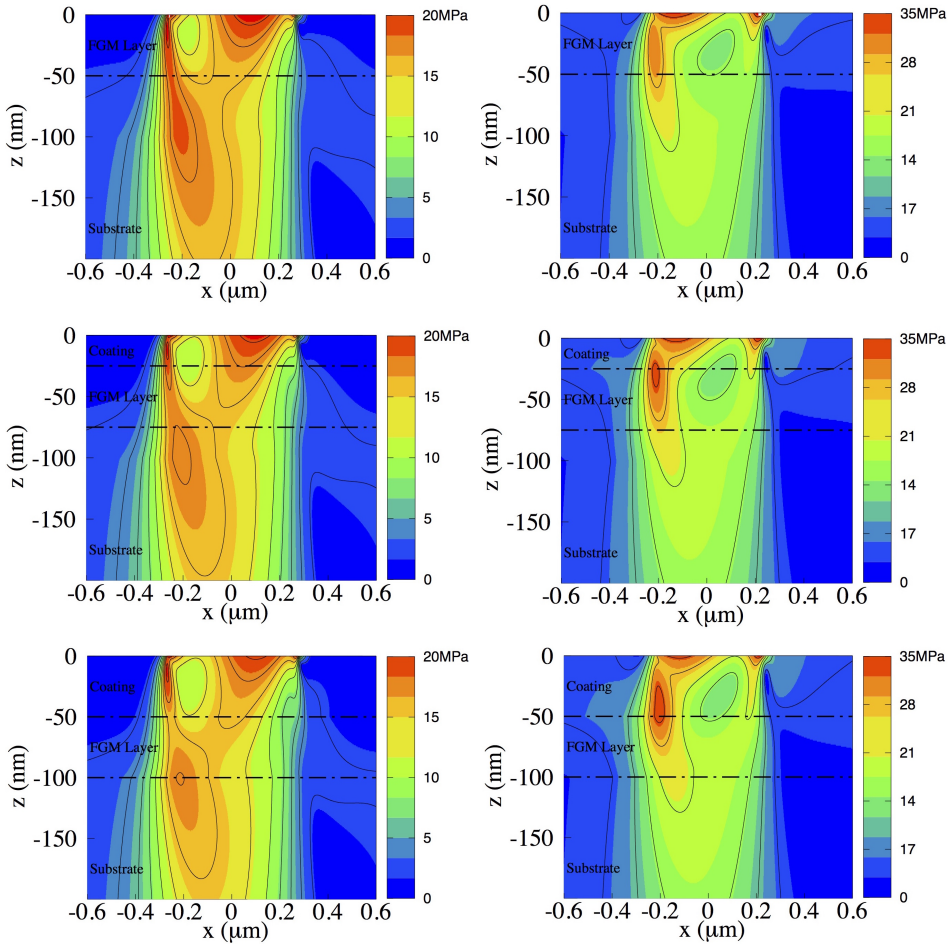

(a) soft coating, $\mu_1/\mu_0 = 0.5$ (b) hard coating, $\mu_1/\mu_0 = 2.0$

Figure 9: Sub-surface stress plots considering coating thickness variation separated from the substrate by a 50nm thick FGM transition layer ($\Delta\gamma = 10\text{mJ}/m^2$, $\eta = 0.4$)

4.5. The effects of transition layer thickness

A further variable of interest in this problem is the thickness of the graded transitional layer. Figure 10 illustrates that increasing thickness of the FGM transitional layer produces a higher peak pressure for the harder coating while the opposite can be observed for the softer coating. It can also be seen that without the FGM transitional layer, a discontinuous stress distribution is experienced by the layered solid (as shown in figure 11(a) and (b)). This is analagous to the results we would expect to see for the case of two

homogeneous yet distinct elastic layers bonded together [34].

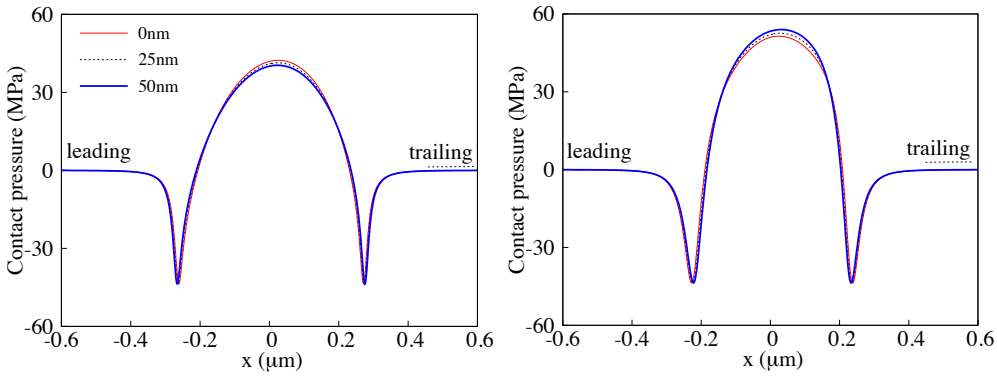

(a) soft coating, $\mu_1/\mu_0 = 0.5$ (b) hard coating, $\mu_1/\mu_0 = 2.0$

Figure 10: Contact behaviour considering FGM layer thickness variation separating the substrate from a 50nm thick coating ($\Delta\gamma = 10\text{mJ}/m^2$, $\eta = 0.4$)

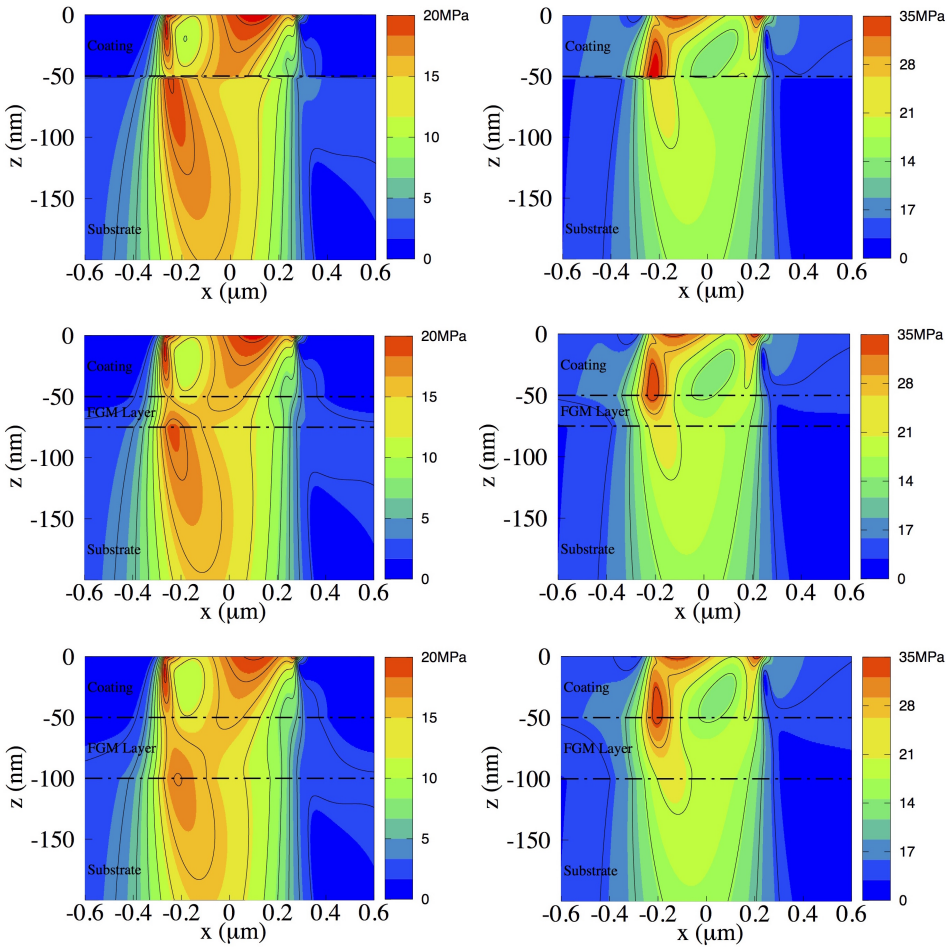

(a) soft coating, $\mu_1/\mu_0 = 0.5$ (b) hard coating, $\mu_1/\mu_0 = 2.0$

Figure 11: Sub-surface stress plots considering FGM layer thickness variation separating the substrate from a 50nm thick coating ($\Delta\gamma = 10\text{mJ}/m^2$, $\eta = 0.4$)

4.6. Modifying the tangential traction

The analysis thus far has assumed Coulombic traction, which may not accurately describe a sliding and adhering contact. This has been discussed by researchers such as Briscoe and Kremnitzer [35] and Thornton [36]. In [37], Derjaguin and Toporov expressed the traction force of adhering contact as:

$$wQ = \eta\,(P + 2P_c) \tag{27}$$

where P is the applied normal load and P_c represents the pull-off force with the condition that $P > -P_c$. Through expansion, equation (27) can be rewritten as:

$$q(x) = \eta p(x) + \tau_0 \tag{28}$$

where τ_0 represents the product of friction coefficient η with the pull-off force, P_c. For a weakly adhering contact, the value of τ_0 will be small in comparison to the applied pressure, making the term negligible. Hence, this will reduce the tangential force to Coulombic traction once again, where $q(x) \approx \eta p(x)$. However, if the term τ_0 is of the same order of magnitude as the contact pressure, $p(x)$, which may be the case for softer substrates, the tractional behaviour of the contact will be significantly influenced by the term τ_0.

The effect of the term τ_0 on the contact pressure and deflection within an adhering contact can be seen in figure 12 for both the hard and soft coatings already considered. Considering similar substrate with Young's modulus of 25GPa, we can see here that as τ_0 becomes larger in magnitude, the distortion of the contact pressure becomes more visible. It is also interesting to note that the trailing edge region of the contact seems to be more attracted to the rigid indenter with higher values of τ_0 for both the hard and soft coating.

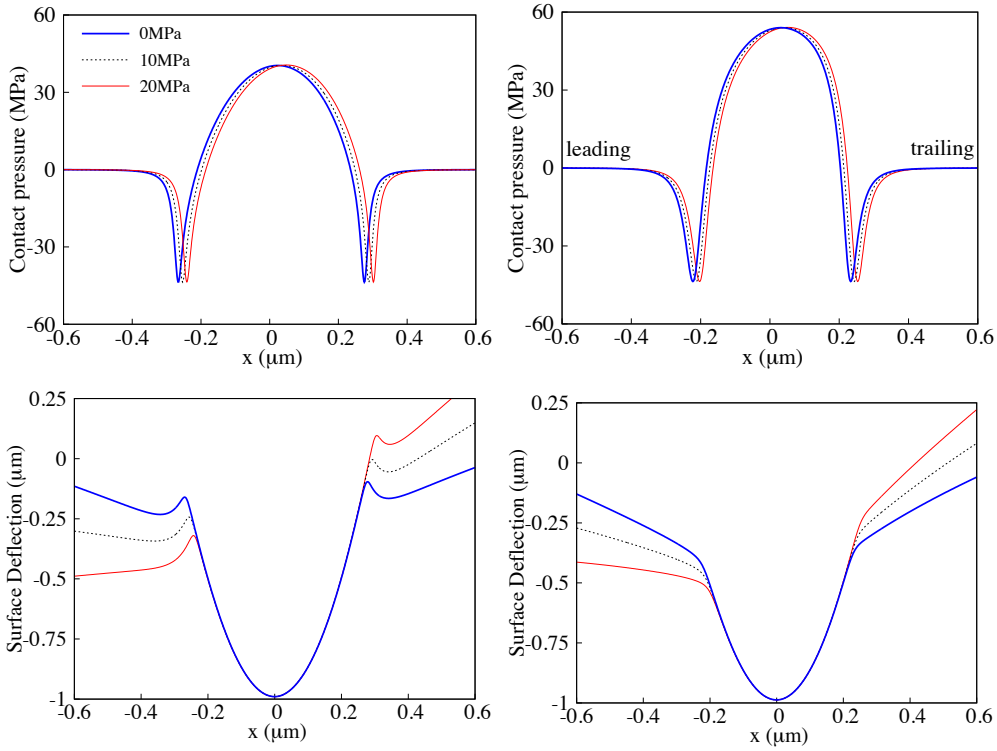

(a) soft coating, $\mu_1/\mu_0 = 0.5$ (b) hard coating, $\mu_1/\mu_0 = 2.0$

Figure 12: Contact characteristics with increasing τ_0 values ($\Delta\gamma = 10\text{mJ}/m^2$, η=0.4)

Figure 13 illustrates the transient behaviour of the location of the highly stressed regions within the layered solid as the value of τ_0 increases. The critical stress values increase when τ_0 increases for both types of coatings. An interesting point to note is that the critically stressed region within the softer coating tends to concentrate close to the trailing edge of the contact. Unlike the softer coating, at more significant τ_0 values, the stress for the harder coating tends to spread sideways, resulting in a larger highly stressed region.

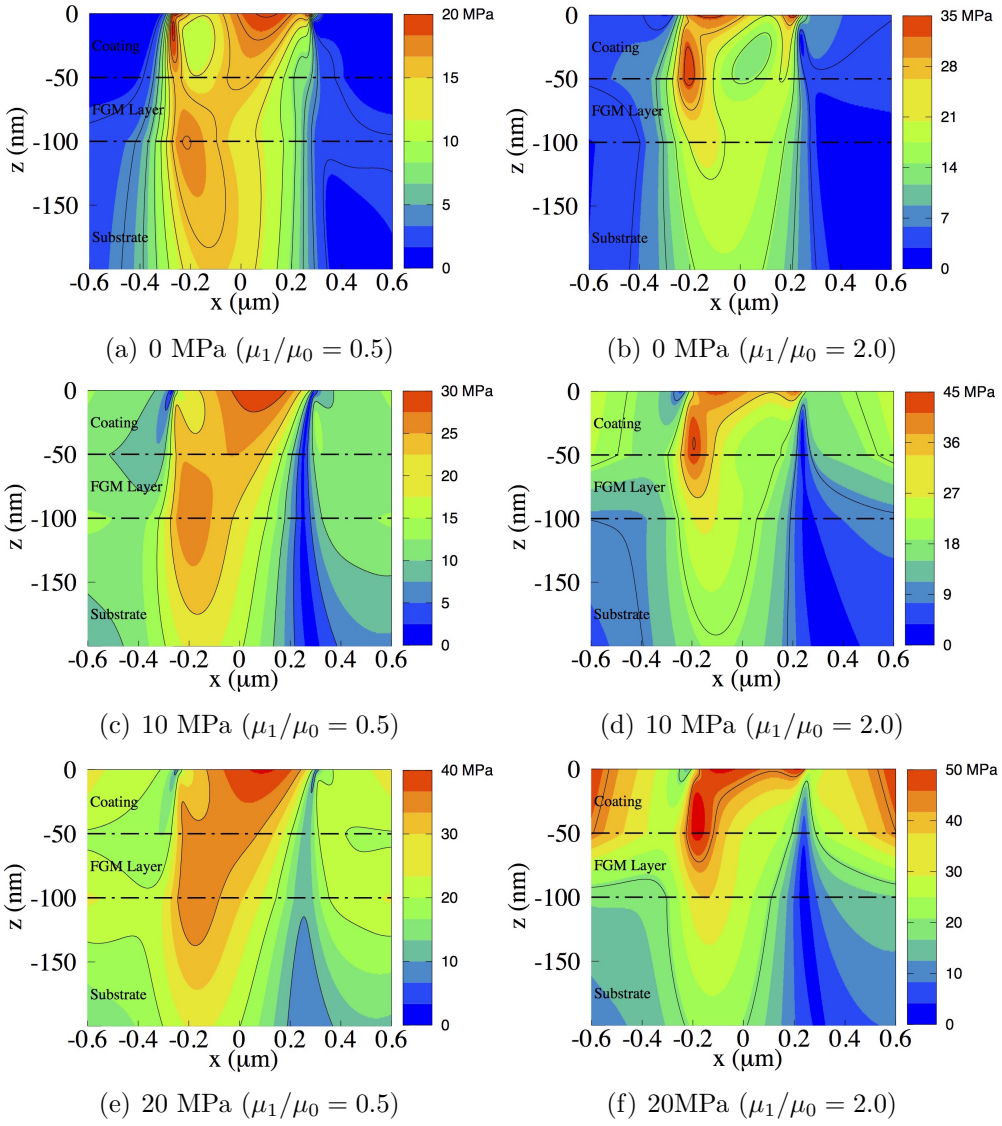

(a) 0 MPa ($\mu_1/\mu_0 = 0.5$)

(b) 0 MPa ($\mu_1/\mu_0 = 2.0$)

(c) 10 MPa ($\mu_1/\mu_0 = 0.5$)

(d) 10 MPa ($\mu_1/\mu_0 = 2.0$)

(e) 20 MPa ($\mu_1/\mu_0 = 0.5$)

(f) 20MPa ($\mu_1/\mu_0 = 2.0$)

Figure 13: Sub-surface stress plots with increasing τ_0 values ($\Delta\gamma = 10\text{mJ}/m^2$, η=0.4)

5. Conclusions

This paper has proposed an iterative algorithm for the solution of the contact problem concerning a rigid indenter sliding over and adhering to the surface of a multi-layered elastic solid. The adhesive forces between the indenter and solid are modelled using the Lennard-Jones potential, whilst the

investigated multi-layered solid consists of a homogeneous coating bonded through a functionally-graded transitional layer to a homogeneous substrate.

A selection of numerical results were presented that demonstrate the significance of the combined effects of traction and boundary adhesion on the layered solid. It was found that hard coatings tend to be more resistant to the applied pressure as the surface displacemant is smaller than that for a soft coating. The maximum principal stress in the hard coating is much larger than that for a soft coating however and regions of very high stress are observed to form beneath the surface. Another interesting finding from the simulation also showed that increasing either the coating or FGM transition layer thickness would result in a reduced peak pressure for a soft coating but otherwise for the hard coating. The observations from the results mean that the likelihood of material wear and possible failure is increased for a hard coating.

Perhaps the most significant observation in this work is that a suitable mathematical representation for the traction distribution along the sliding adhering contact is critical in determining the performance of the layered solid under pressure. The sliding behaviour within this work has been sim-ulated using the assumptions of Coulombic traction and those of [37]. As expected, the obtained results for a weakly adhering contact are very similar in both cases due to the small pull-off force. It is however noted that as the pull-off force increases, the maximum stress in both the hard and soft coating increases and large regions of high stress begin to occur within all three lay-ers of the solid. This indicates that the likelihood of material failure in both hard and soft coatings increases as the contact exhibits stronger adhesion.

The mathematical approach proposed in the paper provides a platform to better understand the combined effects of traction and boundary adhesion for sliding contacts along a multi-layered solid, in order to aid the design of application specific low-wear materials.

Acknowledgement

The authors wish to acknowledge the financial support of Engineering Physical Sciences Research Council (EPSRC) under the ENCYCLOPAEDIC Program Grant, as well as the contributions from industrial partners working on the same project.

References

[1] S. Suresh, M. Olsson, A.E. Giannakopoulos, N.P. Padture, and J. Jitcharoen. Engineering the resistance to sliding-contact damage through controlled gradients in elastic properties at contact surfaces. *Acta Materialia*, 47(14):3915–3926, 1999.

[2] S. Suresh. Graded materials for resistance to contact deformation and damage. *Science*, 292(5526):2447–2451, 2001.

[3] W.W.F. Chong, S. Howell-Smith, M. Teodorescu, and N.D. Vaughan. The influence of inter-ring pressures on piston-ring/liner tribological conjunction. *Proceedings of the Institution of Mechanical Engineers, Part J: Journal of Engineering Tribology*, page 1350650112461579, 2012.

[4] M. De la Cruz, W.W.F. Chong, M Teodorescu, S. Theodossiades, and H. Rahnejat. Transient mixed thermo-elastohydrodynamic lubrication in multi-speed transmissions. *Tribology International*, 49:17–29, 2012.

[5] W.W.F. Chong, M. Teodorescu, and H. Rahnejat. Mixed thermo-elastohydrodynamic cam–tappet power loss in low-speed emission cycles. *International Journal of Engine Research*, page 1468087412461631, 2012.

[6] H. Hertz. On the contact of elastic solids. *J. reine angew. Math*, 92(156-171):110, 1881.

[7] K. L. Johnson, K. Kendall, and A. D. Roberts. Resolving the contradiction of asperities plastic to elastic mode transition in current contact models of fractal rough surfaces. *Proc. Roy. Soc., Series A*, 324:301–313, 1971.

[8] B. V. Derjaguin, V. M. Muller, and Y. P. Toporov. Effect of contact deformation on the adhesion of elastic solids. *J. Colloid and Interface Sci.*, 53:314–326, 1975.

[9] D. Maugis. On the contact and adhesion of rough surfaces. *J. Adhesion Sci. & Tech.*, 10:161–175, 1996.

[10] M. Teodorescu and H. Rahnejat. Mathematical modelling of layered contact mechanics of cam tappet conjunction. *App. Math. Modell.*, 31:2610–2627, 2007.

[11] W.W. Chen, K. Zhou, L.M Keer, and Q.J. Wang. Modeling elasto-plastic indentation on layered materials using the equivalent inclusion method. *International Journal of Solids and Structures*, 47(20):2841–2854, 2010.

[12] C. Yu, Z. Wang, and Q.J. Wang. Analytical frequency response functions for contact of multilayered materials. *Mechanics of Materials*, 76:102–120, 2014.

[13] Z. Wang, C. Yu, and Q.J. Wang. An efficient method for solving three-dimensional fretting contact problems involving multilayered or functionally graded materials. *International Journal of Solids and Structures*, 66:46–61, 2015.

[14] A. E. Giannakopoulos and S. Suresh. Indentation of solids with gradients in elastic properties: Part i. point force. *Int. J. Solids and Struct.*, 34(19):2357–2392, 1997.

[15] M. A. Guler and F. Erdogan. Contact mechanics of graded coatings. *Int. J. Solids and Struct.*, 41(14):3865–3889, 2004.

[16] S. J. Chidlow, M. Teodorescu, and N. D. Vaughan. Predicting the deflection and sub-surface stress field within two dimensional in homogeneously elastic bonded layered solids under pressure. *Int. J. Solids and Struct.*, 48:3243–3256, 2011.

[17] K. L. Johnson and I. Sridhar. Adhesion between a spherical indenter and an elastic solid with a compliant elastic coating. *J. Phy. D: App. Phy.*, 34(5):683, 2001.

[18] P. Mary, A. Chateauminois, and C. Fretigny. Deformation of elastic coatings in adhesive contacts with spherical probes. *J. Phy. D: App. Phy.*, 39(16):3665, 2006.

[19] A.O. Sergici, G.G Adams, and S. Müftü. Adhesion in the contact of a spherical indenter with a layered elastic half-space. *Journal of the Mechanics and Physics of Solids*, 54(9):1843–1861, 2006.

[20] S.J. Chidlow, W.W.F. Chong, and M. Teodorescu. On the two dimensional solution of both adhesive and non-adhesive contact problems involving functionally graded materials. *Eur. J. Mech. A/solids*, 39:86–103, 2013.

[21] W.W.F. Chong and S.J. Chidlow. Modelling adhesive contact problems involving a layered elastic solid and cylindrical indenter using lennard jones potential. *Mechanics of Materials*, 84:1–11, 2015.

[22] G.M. Hamilton and L.E. Goodman. The stress field created by a circular sliding contact. *Journal of Applied Mechanics*, 33(2):371–376, 1966.

[23] H. Poritsky. Stresses and deflections of cylindrical bodies in contact with application to contact of gears and of locomotive wheels. *Journal of Applied Mechanics-Transactions of the ASME*, 17(2):191–201, 1950.

[24] A.E. Giannakopoulos and P. Pallot. Two-dimensional contact analysis of elastic graded materials. *Journal of the Mechanics and Physics of Solids*, 48(8):1597–1631, 2000.

[25] M.A. Guler and F. Erdogan. The frictional sliding contact problems of rigid parabolic and cylindrical stamps on graded coatings. *International journal of mechanical sciences*, 49(2):161–182, 2007.

[26] L. Ke and Y. Wang. Two-dimensional sliding frictional contact of functionally graded materials. *European Journal of Mechanics-A/Solids*, 26(1):171–188, 2007.

[27] S.J. Chidlow and M. Teodorescu. Sliding contact problems involving inhomogeneous materials comprising a coating-transition layer-substrate and a rigid punch. *International Journal of Solids and Structures*, 51(10):1931–1945, 2014.

[28] S. Chen, C. Yan, and A. Soh. Adhesive behavior of two-dimensional power-law graded materials. *International Journal of Solids and Structures*, 46(18):3398–3404, 2009.

[29] K. L. Johnson. *Contact mechanics*. Cambridge university press, 1987.

[30] J.W. Cooley and J.W. Tukey. An algorithm for the machine calculation of complex fourier series. *Mathematics of computation*, 19(90):297–301.

[31] J. Wu. Adhesive contact between a cylinder and a half-space. *Journal of Physics D: Applied Physics*, 42(15):155302, 2009.

[32] M.A. Lantz, S.J. O'shea, M.E. Welland, and K.L. Johnson. Atomic-force-microscope study of contact area and friction on nbse 2. *Physical Review B*, 55(16):10776, 1997.

[33] D. Tabor. Surface forces and surface interactions. *Journal of colloid and interface science*, 58(1):2–13, 1977.

[34] R.B. King and T.C. O'sullivan. Sliding contact stresses in a two-dimensional layered elastic half-space. *International Journal of Solids and Structures*, 23(5):581–597, 1987.

[35] B.J. Briscoe and S.L. Kremnitzer. A study of the friction and adhesion of polyethylene-terephthalate monofilaments. *Journal of Physics D: Applied Physics*, 12(4):505, 1979.

[36] C. Thornton. Interparticle sliding in the presence of adhesion. *Journal of Physics D: Applied Physics*, 24(11):1942, 1991.

[37] J.M. Georges. *Microscopic aspects of adhesion and lubrication*, volume 7. Elsevier, 1982.

Appendix A. Nomenclature

A	Non-dimensional initial state of contact $(-)$
E_0	Young's modulus of the substrate (Pa)
E_1	Young's modulus on the surface of the coating(Pa)
G_0	Shear modulus of the substrate (Pa)
G_1	Shear modulus on the surface of the substrate (Pa)
G	Shear modulus of the functionally graded coating (Pa)
H_c	Non-dimensional undeformed contact geometry $(-)$
H	Non-dimensional contact gap $(-)$
L	Non-dimensional contact width $(-)$
P	Applied normal load (N)
P_c	Pull-off force (N)
Q	Traction force (N)
R	Indenter curvature radius (m)
R_i	Residual term $(-)$
U	Non-dimensional deflection in x-direction $(-)$
V	Non-dimensional deflection in y-direction $(-)$
X	Non-dimensional horizontal co-ordinate $(-)$

Y	Non-dimensional vertical co-ordinate $(-)$
a	Contact half width for Maugis-Dugdale model (m)
b	Equivalent contact half width for Maugis-Dugdale model (m)
c	Outer half width for adhesive region (m)
h	Contact gap (m)
h_c	Rigid indenter geometry (m)
p	Contact pressure (Pa)
u	Deflection in x-direction (m)
v	Deflection in y-direction (m)
x	Horizontal co-ordinate (m)
y	Vertical co-ordinate (m)
Ω	Relaxation term $(-)$
α	Approach of indenter (m)
l	Contact width (m)
ϵ	Atomic equilibrium spacing (m)
ν	Poisson's ratio of the solid $(-)$
σ_{yy}	Normal stress in the y-direction (Pa)
σ_{xx}	Normal stress in the x-direction (Pa)
σ_{xy}	Shear stress (Pa)
τ_1	Principal stress (Pa)

Appendix B. Description of the Mathematical Model

We seek solutions of the stress functions within each region of the solid as indefinite integrals which result from the application of Fourier transforms. The definition of the Fourier transform used within this work is

$$\hat{f}(\xi) = \int_{-\infty}^{\infty} f(x) e^{i\xi x} dx \tag{B.1}$$

where $f(x)$ is an arbitrary function.

Following [27], we find that the solutions of the transformed stress functions are

$$\hat{\phi}_1(\xi, y) = \Big(C_1 + C_2 y\Big) e^{|\xi| y} + (C_3 + C_4 y) e^{-|\xi| y}, \tag{B.2}$$

$$\hat{\phi}_2(\xi, y) = \sum_{n=1}^{4} A_n e^{\lambda_n} y, \tag{B.3}$$

$$\hat{\phi}_3(\xi, y) = \Big(D_1 + D_2 y\Big) e^{|\xi| y} \tag{B.4}$$

where

$$\lambda_1 = \sqrt{\frac{1}{4}\left(\alpha^2+4\xi^2\right)+i\alpha|\xi|\sqrt{\frac{\nu}{1-\nu}}}+\frac{1}{2}\alpha, \tag{B.5}$$

$$\lambda_2 = -\sqrt{\frac{1}{4}\left(\alpha^2+4\xi^2\right)+i\alpha|\xi|\sqrt{\frac{\nu}{1-\nu}}}+\frac{1}{2}\alpha, \tag{B.6}$$

$$\lambda_3 = \bar{\lambda}_1, \tag{B.7}$$

$$\lambda_4 = \bar{\lambda}_2. \tag{B.8}$$

The constants appearing in (B.2) and (B.4) are ξ-dependent and may be computed from the relationships

$$\begin{pmatrix} C_1 \\ C_2 \end{pmatrix} = \Phi^{-1}\begin{pmatrix} \frac{\hat{P}(\xi)}{\xi^2} \\ \frac{i\hat{Q}(\xi)}{\xi} \end{pmatrix}, \tag{B.9}$$

$$\begin{pmatrix} C_3 \\ C_4 \end{pmatrix} = -e^{-2|\xi|h_1}\left(J_1-SW^{-1}L_1\right)^{-1}\left(H_1-SW^{-1}G_1\right)\times \Phi^{-1}\begin{pmatrix} \frac{\hat{P}(\xi)}{\xi^2} \\ \frac{i\hat{Q}(\xi)}{\xi} \end{pmatrix}, \tag{B.10}$$

$$\begin{pmatrix} A_1 \\ A_3 \end{pmatrix} = W^{-1}\left(e^{-|\xi|h_1}G_1\begin{pmatrix} C_1 \\ C_2 \end{pmatrix}+e^{|\xi|h_1}L_1\begin{pmatrix} C_3 \\ C_4 \end{pmatrix}\right), \tag{B.11}$$

$$\begin{pmatrix} A_2 \\ A_4 \end{pmatrix} = -\left(T_2K_2^{(2)}\right)^{-1}T_1K_1^{(2)}\begin{pmatrix} A_1 \\ A_3 \end{pmatrix}, \tag{B.12}$$

$$\begin{pmatrix} D_1 \\ D_2 \end{pmatrix} = e^{|\xi|h_2}G_2^{-1}\left(M_1K_1^{(2)}\begin{pmatrix} A_1 \\ A_3 \end{pmatrix}+M_2K_2^{(2)}\begin{pmatrix} A_2 \\ A_4 \end{pmatrix}\right). \tag{B.13}$$

The 2×2 matrices appearing above are defined as

$$K_j^{(i)} = \begin{pmatrix} e^{-\lambda_j h_i} & 0 \\ 0 & e^{-\bar{\lambda}_j h_i} \end{pmatrix}, \tag{B.14}$$

$$N_j = \begin{pmatrix} 1 & 1 \\ \lambda_j & \bar{\lambda}_j \end{pmatrix}, \tag{B.15}$$

$$M_j = \begin{pmatrix} \mathcal{F}(\lambda_j) & \mathcal{F}(\bar{\lambda}_j) \\ \mathcal{G}(\lambda_j) & \mathcal{G}(\bar{\lambda}_j) \end{pmatrix}, \tag{B.16}$$

$$H_j = \begin{pmatrix} 1 & -h_j \\ |\xi| & 1 - |\xi| h_j \end{pmatrix}, \tag{B.17}$$

$$J_j = \begin{pmatrix} 1 & -h_j \\ -|\xi| & 1 + |\xi| h_j \end{pmatrix}, \tag{B.18}$$

$$G_j = \begin{pmatrix} \xi^2 & 2(1-\nu)|\xi| - \xi^2 h_j \\ -|\xi|\xi^2 & \xi^2\big((1-2\nu) + |\xi| h_j\big) \end{pmatrix}, \tag{B.19}$$

$$L_j = \begin{pmatrix} \xi^2 & -\big(2(1-\nu)|\xi| + \xi^2 h_j\big) \\ |\xi|\xi^2 & \xi^2\big((1-2\nu) - |\xi| h_j\big) \end{pmatrix}, \tag{B.20}$$

$$\Phi = H_0 - e^{-2|\xi|h_1} J_0 \left(J_1 - S W^{-1} L_1\right)^{-1} \left(H_1 - S W^{-1} G_1\right), \tag{B.21}$$

$$S = N_1 K_1^{(1)} - N_2 K_2^{(1)} \left(T_2 K_2^{(2)}\right)^{-1} T_1 K_1^{(2)}, \tag{B.22}$$

$$W = M_1 K_1^{(1)} - M_2 K_2^{(1)} \left(T_2 K_2^{(2)}\right)^{-1} T_1 K_1^{(2)}, \tag{B.23}$$

$$T_j = N_J - H_2 G_2^{-1} M_j \tag{B.24}$$

for $i, j = 1, 2$, whilst

$$\hat{P}(\xi) = \int_{-\infty}^{\infty} p(x) e^{i\xi x} dx = \int_{-b}^{a} p(x) e^{i\xi x} dx, \tag{B.25}$$

$$\hat{Q}(\xi) = \int_{-\infty}^{\infty} q(x) e^{i\xi x} dx = \int_{-b}^{a} q(x) e^{i\xi x} dx \tag{B.26}$$

are the Fourier transforms of the contact pressure and tangential traction. The functions appearing in (B.16) are defined as

$$\mathcal{F}(\lambda_j) = (1-\nu)\lambda_j^2 + \nu\xi^2, \tag{B.27}$$

$$\mathcal{G}(\lambda_j) = (1-\nu)\lambda_j^3 - \alpha(1-\nu)\lambda_j^2 - \xi^2(2-\nu)\lambda_j - \alpha\nu\xi^2. \tag{B.28}$$

The notation $h_0 = 0$ has been adopted here to denote the solid surface, whilst h_1 and h_2 represent the interface between the coating and transition layer and transition layer and substrate respectively.

Appendix C. List of the non-dimensionalisations used within this work

$$
\begin{aligned}
H &= h/\epsilon - 1 \\
H_c &= h_c/\epsilon \\
\Delta_c &= \alpha/\epsilon \\
U &= u/\epsilon \\
V &= v/\epsilon \\
X &= x/\sqrt{\epsilon R} \\
Y &= Y/\sqrt{\epsilon R} \\
L &= \ell/\sqrt{\epsilon R} \\
\mu &= [R\gamma^2/(E^2\epsilon^3)]^{1/3} \\
\frac{1}{E} &= \frac{1-\nu_0^2}{E_0} + \frac{1-\nu_1^2}{E_1}
\end{aligned}
$$

Appendix D. Simulation Parameters

	Parameters	**Values**	**Units**
1.	R_x	40	μm
2.	ϵ	0.235	nm
3.	ν	0.26	-
4.	h_1	50	nm
5.	h_2	100	nm
6.	δ_{max}	0.1	nm